We are IntechOpen, the world's leading publisher of Open Access books Built by scientists, for scientists

6,900
Open access books available

185,000
International authors and editors

200M
Downloads

Our authors are among the

154
Countries delivered to

TOP 1%
most cited scientists

12.2%
Contributors from top 500 universities



WEB OF SCIENCE™

Selection of our books indexed in the Book Citation Index in Web of Science™ Core Collection (BKCI)

Interested in publishing with us?
Contact book.department@intechopen.com

Numbers displayed above are based on latest data collected.
For more information visit www.intechopen.com



8

Simulation of Acoustic Sound Produced by Interaction Between Vortices and Arbitrarily Shaped Body in Multi-Dimensional Flows by the Vortex Method

Yoshifumi Ogami
Ritsumeikan University
Japan

1. Introduction

One of the most important environmental and/or engineering issues at present is the reducing aerodynamic noise that is produced from, for example, the body surfaces of cars; parts of cars, such as sideview mirrors, windshield wipers, and roof racks; pantographs of bullet trains; narrow spaces between cars of bullet trains; and fans in air-conditioners.
In order to analyze aerodynamic sound for practical engineering use, the decoupled solution method—which treats the flow field and acoustic field separately—has been employed. In this method, the flow field involves an inviscid incompressible fluid that yields a sound source, and the acoustic field is analyzed by combining this source with wave equations, such as the Lighthill equation. Powell (1964) and Howe (2003) showed that this sound source is represented by a vorticity vector. Therefore, aerodynamic sound is considered to originate from the unsteady motion of vorticity; that is, generation and deformation of vorticity, accelerated motion of vorticity, interaction of vorticity, and interference of obstacles. This chapter mainly focuses on the simulation of vortex sounds created by obstacle interference in multi-dimensional flows through the simple but powerful vortex method.
Using the compact Green's function, which is based on the compact assumption that the wavelength of sound is large compared to the dimensions of the solid body, Howe (2003) studied the vortex sound for one of the most fundamental cases of interference: namely, where one vortex line passes near an obstacle. In this study, the vortex movement was calculated based on the potential flow of the inviscid and incompressible fluid so that the computational load and time would be very small. The fundamental aspects of the sound produced by an interaction between vorticity and obstacle are well understood. However, the obstacles are limited to two-dimensional simple shapes because the conformal mappings to create the obstacles have to be known.
Therefore, this chapter presents a generalization of Howe's method to treat two-dimensional shapes with unknown conformal mappings and three-dimensional obstacles in as simple manner as possible. This generalization will help in analyzing the sound produced by vorticity and an arbitrarily shaped body with less computational effort for studying the effect of the body shape on the aerodynamic sound, controlling the aerodynamic sound, etc.
To calculate the flow fields in two and three dimensions, we employ the vortex method

(panel method), which can directly and easily deal with an arbitrarily shaped body with vortices in non-linear motion.

The vortex method has been used to analyze aerodynamic sounds through the various equations or methods listed below:

1. Sharland's equation that relates the lift coefficient to sound power (Sharland, 1964).
2. Curl's equation that calculates the aerodynamic sound from the pressure fluctuations on the surface of a body (Curle, 1955).
3. The Ffowcs Williams–Hawkings equation that treats the aerodynamic sound of rotating wings (Ffowcs Williams & Hawkings, 1969, Huberson et al., 2008).
4. The asymptotic matching method and panel method (Kao, 2002).
5. Howe's method with the compact Green's function (Howe, 2003).

Of these methods, Howe's method provides a simple and direct relation between the vortex sound and vortex. Ogami and Akishita (2010) applied Howe's method to the aerodynamic sound produced by the interaction of a flat plate and vortices in non-linear motion. The relation between the acoustic pressure and vortices is directly expressed in a simple manner so that the effects of the vortices in non-linear motion on the acoustic sound can be studied easily with less computational effort than the other methods. As stated before, one of the purposes of this chapter is to generalize Howe's method to treat two-dimensional shapes with unknown conformal mappings and three-dimensional obstacles; the details are explained in Section 2. The idea for calculating the acoustic pressure of arbitrarily shaped obstacles without conformal mappings is to use three sets of bound vortices that represent the obstacles in uniform flows of speed 1 in the x and y directions in two dimensions as well as in the z-direction in three dimensions. These bound vortices are obtained by the panel method in advance.

To examine the validity and accuracy of our method, we compared our solutions with those of Howe for the acoustic pressure produced by the interaction of an incident vortex and circular cylinder, and we present our findings in Section 3.

Howe (1976) showed that *the imposition of a Kutta condition at the trailing edge leads to a complete cancellation of the sound generated when frozen turbulence (the turbulence is modeled by a line vortex convected in a mean flow) convects past a semi-finite plate and to the cancellation of the diffraction field produced by the trailing edge in the case of an airfoil of compact chord.* However, his results were based on the linear assumption that the strength of the incident vortex is small enough so that its path is almost linear and that the wake vortices are also swept downstream at the mean stream velocity. Since our method is applicable to non-linear simulations where the wake vortices are swept at velocities induced by other vortices, both an airfoil (Section 3) and semi-finite plate (Section 4) were considered with fully non-linear calculations. The shedding of wake vortices was found to not cancel the sound but has the extra effect of producing sound due to the accelerated movements of the wake vortices.

Our findings were also compared with Kao's solutions by the asymptotic matching method, as presented in Section 4. Our solutions are considerably simpler and easier to code than those of Kao's analysis.

Section 5 discusses the sound produced by the vortex motion near a half-plane to study the effect of shedding vortices from the edge on the sound. Section 6 presents the study of a three-dimensional rectangular solid for examining the effect of three-dimensionality for an incident vortex on the vortex sound. The shedding of wake vortices was not considered.

In this study, two types of vortices were used: the free vortex and the bound vortex. The movements of the free vortices, which were the sources of the sound, were calculated on the basis of the potential flow of the inviscid and the incompressible fluid as stated before. The bound vortices were used for representing an arbitrarily shaped body. This body can be created in the potential flow by adjusting the strengths of the bound vortices, which were arranged on the virtual panels placed along the body, under the non-permeable condition that the stream line does not penetrate this body.

2. Acoustic pressure for arbitrarily shaped bodies with free vortices in non-linear motion

As stated in the Introduction, Howe's solutions (2003) are limited to body shapes whose conformal mappings are known. In this section, we derive the relations between the acoustic pressures in the two-, quasi three-, and three-dimensions and the vortices for interactions with arbitrarily shaped obstacles.

2.1 Two dimensions

Consider the following wave equation:

$$\left(\frac{1}{c^2}\frac{\partial^2}{\partial t^2}-\nabla^2\right)\frac{p(\boldsymbol{x},t)}{\rho}=\mathrm{div}(\boldsymbol{\omega}\wedge\boldsymbol{v}) \tag{1}$$

where c is the sound velocity in the fluid, $p(\boldsymbol{x},t)$ is the acoustic pressure at the observation location $\boldsymbol{x}$ and time t, ρ is the fluid density, and $\boldsymbol{\omega}$ is the vortex vector swept at velocity vector $\boldsymbol{v}$. Using this equation, Howe derived the acoustic pressure $p(\boldsymbol{x},t)$ produced by a vortex of strength Γ located at (x_{01},x_{02}) in a two-dimensional flow as follows:

$$p(\boldsymbol{x},t)=\frac{-\rho\Gamma x_j}{2\pi\sqrt{2c}\,|\,\boldsymbol{x}\,|^{\frac{3}{2}}}\frac{\partial}{\partial t}\int_{-\infty}^{t-|\boldsymbol{x}|/c}\left\{\frac{dx_{01}}{d\tau}\frac{\partial Y_j}{\partial y_2}-\frac{dx_{02}}{d\tau}\frac{\partial Y_j}{\partial y_1}\right\}\frac{d\tau}{\sqrt{t-\tau-|\,\boldsymbol{x}\,|/c}} \tag{2}$$

where Y_j is the component of the Kirchhoff vector $\boldsymbol{Y}$, which depends on the shape of the body and is considered to be a velocity potential with unit speed in the j direction. Note that the coordinates $\boldsymbol{x}$ and x_j denote the position of the observer, whereas (x_{01},x_{02}) indicate the position of the incident vortex.

For the vortex method (panel method), Eq. (2) can be rewritten as explained below.

In a two-dimensional potential flow with unit speed in the x direction and an arbitrarily shaped body represented by bound vortices of strength $\Gamma_{\boldsymbol{Bi}}^{\boldsymbol{X}}$ (the subscript X denotes the the x direction, and B_i indicates the i-th bound vortex), the complex potential, F, and velocity potential, ϕ, are given by

$$F=Uz+\sum_{i=1}^{N}\frac{i\Gamma_{Bi}^{X}}{2\pi}\log(z-z_i) \tag{3}$$

$$\phi=Y_1=Ux-\sum_{i=1}^{N}\frac{\Gamma_{Bi}^{X}}{2\pi}\theta_i \qquad (\ \theta_i \text{ is argument of } z-z_i) \tag{4}$$

Similarly, for a potential flow with unit speed in the y direction and bound vortices of strength Γ_{Bi}^{Y}, the equations are

$$F = Uze^{-i\frac{\pi}{2}} + \sum_{i=1}^{N} \frac{i\Gamma_{Bi}^{Y}}{2\pi} \log(z - z_i) \tag{5}$$

$$\phi = Y_2 = Uy - \sum_{i=1}^{N} \frac{\Gamma_{Bi}^{Y}}{2\pi} \theta_i \tag{6}$$

By using Eqs. (2), (4) and (6), we get the equation below, which directly relates the acoustic pressure to the vortices.

$$p(\boldsymbol{x},t) = \sum_{j=1}^{M} \frac{\rho_0 \Gamma_{Fj} x_1}{2\pi\sqrt{2c_0}\,|\,\boldsymbol{x}\,|^{\frac{3}{2}}} \frac{\partial}{\partial t} \int_{-\infty}^{t-|\boldsymbol{x}|/c_0} \left\{ u_{Fj} \sum_{i=1}^{N} \frac{\Gamma_{Bi}^{X}}{2\pi} \frac{x_j - x_i}{\left(x_j - x_i\right)^2 + \left(y_j - y_i\right)^2} + v_{Fj} \left(1 + \sum_{i=1}^{N} \frac{\Gamma_{Bi}^{X}}{2\pi} \frac{y_j - y_i}{\left(x_j - x_i\right)^2 + \left(y_j - y_i\right)^2} \right) \right\} \frac{d\tau}{\sqrt{t - \tau - |\,\boldsymbol{x}\,|/c_0}}$$

$$+ \sum_{j=1}^{M} \frac{\rho_0 \Gamma_{Fj} x_2}{2\pi\sqrt{2c_0}\,|\,\boldsymbol{x}\,|^{\frac{3}{2}}} \frac{\partial}{\partial t} \int_{-\infty}^{t-|\boldsymbol{x}|/c_0} \left\{ u_{Fj} \left(-1 + \sum_{i=1}^{N} \frac{\Gamma_{Bi}^{Y}}{2\pi} \frac{x_j - x_i}{\left(x_j - x_i\right)^2 + \left(y_j - y_i\right)^2} \right) + v_{Fj} \sum_{i=1}^{N} \frac{\Gamma_{Bi}^{Y}}{2\pi} \frac{y_j - y_i}{\left(x_j - x_i\right)^2 + \left(y_j - y_i\right)^2} \right\} \frac{d\tau}{\sqrt{t - \tau - |\,\boldsymbol{x}\,|/c_0}} \tag{7}$$

where Γ_{Fj} and (u_{Fj}, v_{Fj}) represent the j-th free vortex and its velocity components. The bound vortices Γ_{Bi}^{X} and Γ_{Bi}^{Y} are obtained in advance by the panel method. The first term of the right-hand side of Eq. (7) is called the acoustic pressure of the *drag dipole* (*suction dipole*), and the second term is that of the *lift dipole*. Note that an integral from $-\infty$ to $t-|\,\boldsymbol{x}\,|/c_0$ and a time-derivative remain in the solution (7). These operations are numerically calculated in this chapter.

2.2 Quasi three dimensions

Howe derived the acoustic pressure $p(\boldsymbol{x},t)$ produced by vortex vector $\boldsymbol{\omega}$ located at $\boldsymbol{y}$ in a three-dimensional flow as follows.

$$p(\boldsymbol{x},t) = \frac{-\rho_0 x_j}{4\pi c_0 |\,\boldsymbol{x}\,|^2} \frac{\partial}{\partial t} \int (\boldsymbol{\omega} \wedge \boldsymbol{v}) \left(\boldsymbol{y}, t - \frac{|\,\boldsymbol{x}\,|}{c_0} \right) \cdot \nabla Y_j(\boldsymbol{y}) d^3 y \tag{8}$$

Following Howe's analysis, we assume that a line vortex that interacts with a body remains rectilinear as when it is introduced in the flow. This enables us to use the two-dimensional velocity potential for this analysis, even though the body and the flow are three-dimensional. Therefore, the solutions for this section are considered to be quasi three-dimensional. Fully three-dimensional analysis, where the vortex changes its shape, is introduced in the next section.

When the span of the body in the z direction is L (Fig. 1), the components of the Kirchhoff vector are

$$\begin{aligned} Y_1 &= y_1 - \sum_{i=1}^{N} \frac{\Gamma_{Bi}^X}{2\pi}\theta_i \\ Y_2 &= \begin{cases} y_2 - \sum_{i=1}^{N} \frac{\Gamma_{Bi}^Y}{2\pi}\theta_i & |y_3| < \frac{1}{2}L \\ y_2 & |y_3| > \frac{1}{2}L \end{cases} \\ Y_3 &= y_3 \end{aligned} \tag{9}$$

Using the Dirac delta function δ, the vortex vector is expressed as

$$\boldsymbol{\omega} = (0, 0, \Gamma_{Fj}\delta(y_1 - \int u dt)\delta(y_2 - \int v dt)) \tag{10}$$

where Γ_{Fj} is the strength of the j-th line vortex.

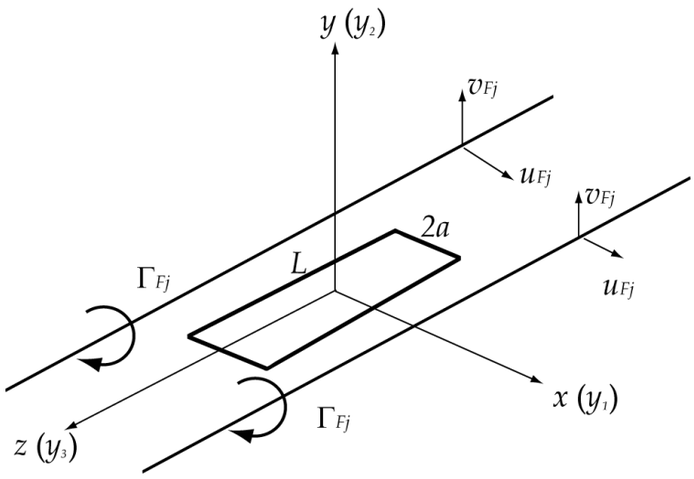


Fig. 1. Coordinate system.

Eqs. (9) and (10) are substituted into Eq. (8) to obtain

$$\begin{aligned} p(\boldsymbol{x},t) = \sum_{j=1}^{M} \frac{\rho_0 x_1 L}{4\pi c_0 |\boldsymbol{x}|^2} \frac{\partial}{\partial t}\Gamma_{Fj} \Bigg\{ & v_{Fj}\left(1 + \sum_{i=1}^{N} \frac{\Gamma_{Bi}^X}{2\pi} \frac{y_j - y_i}{(x_j - x_i)^2 + (y_j - y_i)^2}\right) \\ & + u_{Fj}\left(\sum_{i=1}^{N} \frac{\Gamma_{Bi}^X}{2\pi} \frac{x_j - x_i}{(x_j - x_i)^2 + (y_j - y_i)^2}\right)\Bigg\} \\ + \frac{\rho_0 x_2 L}{4\pi c_0 |\boldsymbol{x}|^2} \frac{\partial}{\partial t}\Gamma_{Fj} \Bigg\{ & v_{Fj}\left(\sum_{i=1}^{N} \frac{\Gamma_{Bi}^Y}{2\pi} \frac{y_j - y_i}{(x_j - x_i)^2 + (y_j - y_i)^2}\right) \\ & - u_{Fj}\left(1 - \sum_{i=1}^{N} \frac{\Gamma_{Bi}^Y}{2\pi} \frac{x_j - x_i}{(x_j - x_i)^2 + (y_j - y_i)^2}\right)\Bigg\} \end{aligned} \tag{11}$$

where the first term of the right-hand side of Eq.(11) is called the acoustic pressure of *drag dipole* (s*uction dipole*) and the second term that of *lift dipole*. As in the two-dimensional analysis, the acoustic pressure is expressed with the free vortices, and with the bound vortices Γ_{Bi}^{X} and Γ_{Bi}^{Y} that are to be obtained in advance by the panel method. Note that the integral that appeard in Eq. (7) does not appear in Eq.(11) but the time-derivative remains.

2.3 Three dimensions

In three dimensions, the acoustic pressure can be calculated directly if the bound vortices Γ_{Bi}^{j}, representing the body within the unit flow in the *j*-direction (*j* = *x*, *y*, and *z*), are obtained in advance. In terms of the velocity vector (u_{Bj}, v_{Bj}, w_{Bj}) produced by the bound vortices Γ_{Bi}^{j} and unit flow in the *j*-direction, the components of the Kirchhoff vector are written as

$$\nabla Y_j(\boldsymbol{y}) = (u_{Bj}, v_{Bj}, w_{Bj}) \tag{12}$$

Therefore, the following term in Eq. (8) can be expressed as

$$(\boldsymbol{\omega} \wedge \boldsymbol{v}) \cdot \nabla Y_j(\boldsymbol{y}) = (\omega_2 w - \omega_3 v,\ \omega_3 u - \omega_1 w,\ \omega_1 v - \omega_2 u) \cdot (u_{Bj}, v_{Bj}, w_{Bj}) \tag{13}$$

Using the free vortices (incident vortex and wake vortices) numbered with *i*, Eq. (8) is expressed as

$$p(\boldsymbol{x}, t) = \frac{-\rho_0 x_j}{4\pi c_0 |\boldsymbol{x}|^2} \frac{\partial}{\partial t} \sum_{i=1}^{N} (\boldsymbol{\Gamma}_i \wedge \boldsymbol{v}) \cdot \nabla Y_j \tag{14}$$

where $\boldsymbol{\Gamma}_i$ is the strength vector of the vorticity vector $\boldsymbol{\omega}_i$ in volume d^3y .

3. Panel method and circular cylinder

3.1 Panel method for acoustic pressure

As shown in Fig. 2, the obstacle in the two-dimensional flow is represented by the discrete bound vortices of strength Γ_{Bi} (dots), and the strength is determined by the non-permeable condition that the components of the fluid velocities normal to the body surface (to the points between the bound vortices (stars) in this study) are zero. The total strength of the bound vortices is assumed to be zero. When there is more than one free vortex in the flow, the strength of the bound vortices varies with the influence of the moving free vortices, so the strength of the bound vortices must be calculated for every time step. On the other hand, the strengths of the bound vortices Γ_{Bi}^{X} and Γ_{Bi}^{Y} in Eqs. (7) and (11) are only obtained once because there is no need to consider the influence of the free vortices for these bound vortices.

3.2 Comparison with Howe's solutions

The acoustic pressure produced by the interaction of a free vortex (incident vortex) and circular cylinder with radius 1 in a uniform flow of velocity 1 was considered. The cylinder was represented by 80 bound vortices. An incident vortex of strength -4π was placed at time 0 at the position *x* = -10, *y* = -0.7. The Adams-Bashforth method of second order accuracy was used to update the position of the incident vortex at time steps of 0.01. The acoustic pressure was calculated by using Eq. (7) for the two-dimensional analysis. The

integral from $-\infty$ to $t-|x|/c_0$ in Eq. (7) was evaluated numerically from a negative value of sufficiently large absolute value to the present time.

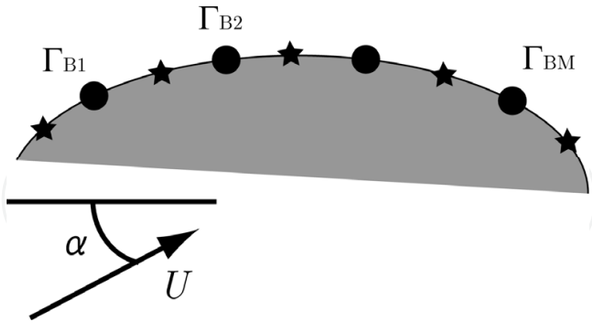


Fig. 2. Positions of bound vortices (dots) and for non-permeable condition (stars).

Figure 3 compares the paths of the incident vortex according to Howe's solution (p. 196, Howe, 2003) and the present method. The incident vortex first placed in the third quadrant at x = -10, y = -0.7 exited this quadrant and entered the second quadrant as it approached the cylinder, flowed along the cylinder surface, and was swept downstream. Although this movement was caused by the effect of the mirror image vortex, the bound vortices placed along the cylinder surface had this effect without the placement of an image vortex inside the cylinder. The paths of both solutions shown in Fig. 3 agreed well, with an average relative error of 0.05%.

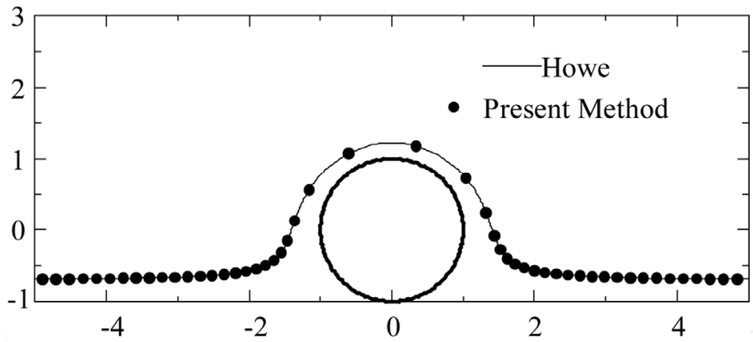


Fig. 3. Path of incident vortex.

The average relative error is defined by Eq.(15),

$$\text{Error} = \frac{1}{n}\sum_{i=1}^{n}\left|\frac{S_{Howe}^{i} - S_{P}^{i}}{S_{MAX}}\right| \times 100\% \tag{15}$$

where S_{Howe}^{i} and S_{P}^{i} are Howe's solution and that of the present method, respectively, at the i-th time step, $|S_{MAX}|$ is the maximum absolute value during the period of calculation, and n is the number of solutions obtained during this period.

Figure 4 compares the acoustic pressures of the drag dipole and lift dipole, as calculated by Howe's method (solid and broken lines) and the present method (dots). The average relative error was 0.3%. According to Howe (2003), the time was set to zero when the incident vortex

passed the position x = 0. The parameters in Fig. 4 are $V = \Gamma / (2\pi a)$ and $a = 1$. The acoustic pressures of the drag and lift dipoles are non-dimensionalized by $k \sin\Theta$ and $k \cos\Theta$, respectively, where $k = \rho_0 V^2 \sqrt{M} \sqrt{a / |\mathbf{x}|}$, $M = V / c_0$, and $\Theta = \tan^{-1}(x_1 / x_2)$.

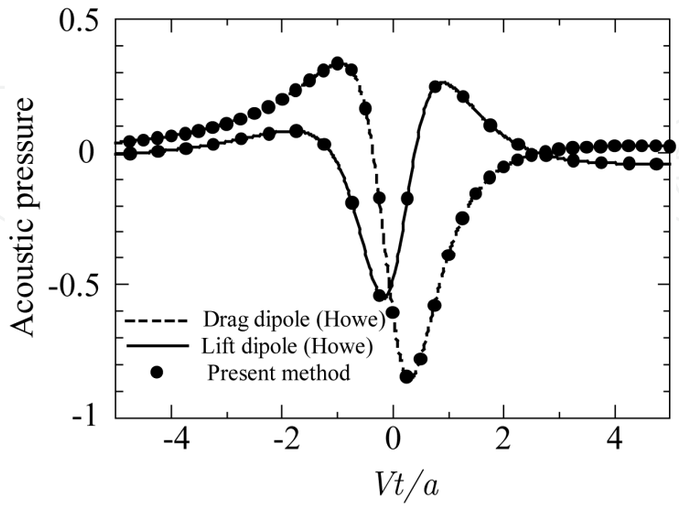


Fig. 4. Drag dipole and lift dipole for the circular cylinder.

Next, to determine the convergence and accuracy of the present method, the acoustic pressure by the drag dipole was calculated while changing the bound vortex number N and time step Δt. Figure 5 shows that for $N > 40$, the average relative error decreased with decreasing time step, and the difference between $N = 80$ and 120 was not noticeable; thus the solutions were considered to converge at $N \geq 80$. The error of the lift dipole had a similar tendency, so that figure is omitted.

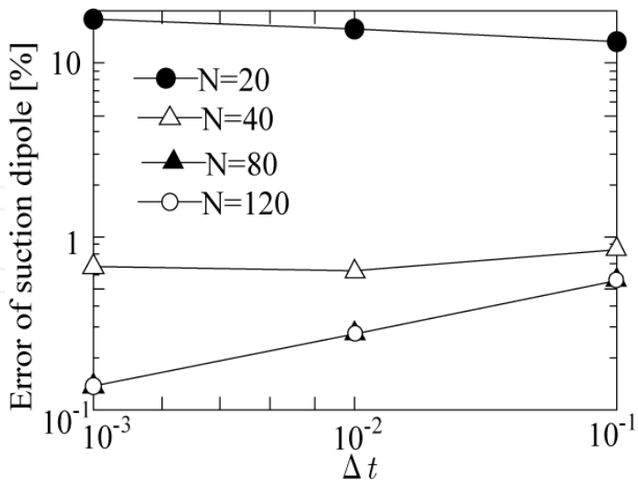


Fig. 5. Averaged relative error for drag dipole.

Figure 6 shows the average relative error for the paths of the incident vortices. The solutions converged with a smaller numbers of bound vortices ($N \geq 40$) than the acoustic pressure in Fig. 5 ($N \geq 80$).

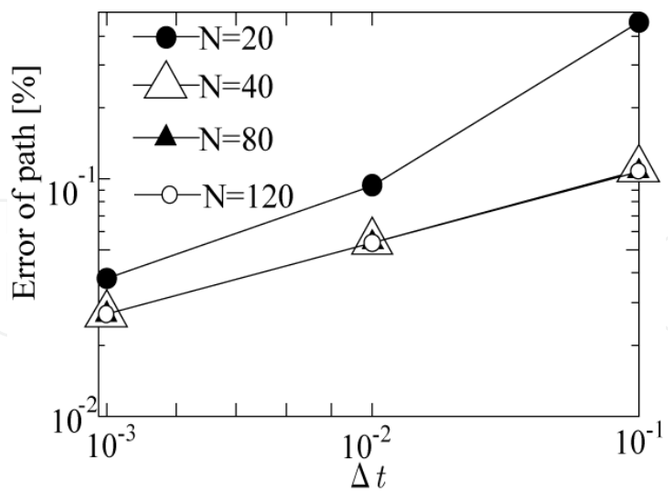


Fig. 6. Averaged relative error for path of the incident vortex.

For the simulations of engineering applications, multiple vortices passing the body and produced on the body surface have to be considered. The acoustic pressure is easily obtained from Eqs. (7) and (11) by summing the acoustic pressures produced by each vortex passing the body. Therefore, although the solutions shown in Fig. 4 are very elemental, they are important for studying the fundamental characteristics of vortex sound.

4. NACA0012 airfoil

4.1 Without wake vortices

As stated before, Howe reported that the wake vortex shed from the trailing edge of an airfoil cancels the acoustic pressure when the Kutta condition is employed. To verify this cancellation, we studied the effect of the wake vortices shed from the NACA0012 airfoil on the acoustic pressure. The airfoil was placed in a uniform flow of velocity 1 and was represented by 160 bound vortices; its leading edge lay at x = 0, and the trailing edge was at x = 1. The angle of attack was set to zero. The incident vortex of strength $\Gamma = -0.4\pi$ started at the position x = -10, y = 0. The time step was set to 0.01.

With the Kutta condition that the flow separates from the trailing edge, wake vortices were produced by the influence of the incident vortex even when the angle of attack was zero. We neglect the production of the wake vortices in this section and consider it in the next section. In addition to the Kutta condition, the total strength of the bound vortices was set to zero for the former case, and the total strength of the bound and wake vortices was set to zero for the latter case.

Figure 7, which is enlarged in the y direction, shows the path of the incident vortex when the production of the wake vortices was not considered. The incident vortex started at x = -10, y = 0, and as it approached the airfoil it was swept upward by the effect of the mirror image vortex. The path broke near the trailing edge, around positions D and E in Fig. 7, because the velocity at the trailing edge was very large (without the Kutta condition, the velocity in the analytical solution becomes infinity). The letters A–E indicate the positions of

the incident vortex when its acceleration, shown in Fig. 9, reached the peak value, and the numbers in parentheses in Fig. 7 are the times of the peak.

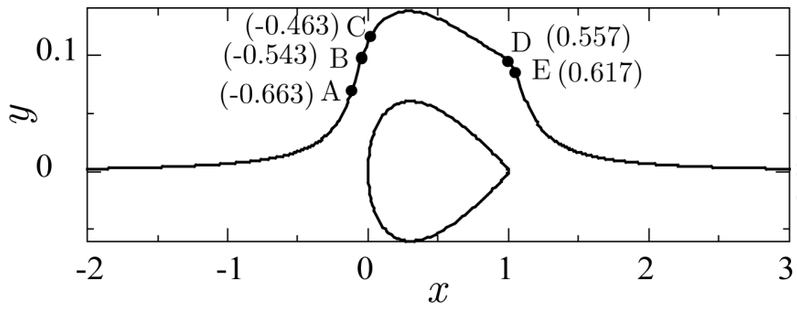
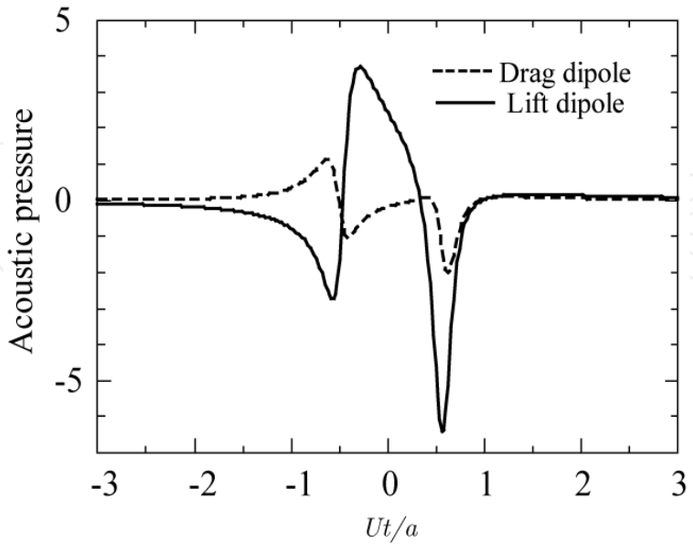


Fig. 7. Path of incident vortex around the NACA0012 airfoil.

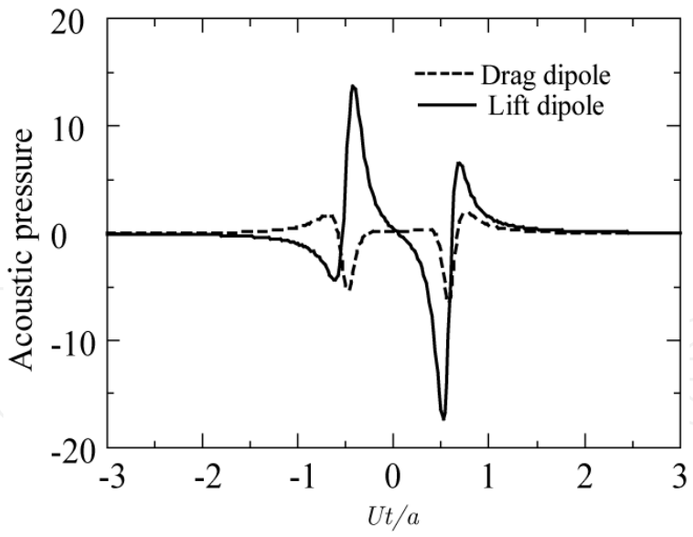
Figure 8 shows the acoustic pressure calculated (a) by Eq. (7) for two-dimensional analysis and (b) calculated by Eq. (11) for quasi three dimensions. The time was set to zero when the incident vortex passed the center of the airfoil (x = 0.5) and was non-dimensionalized as Ut/a (U = 1 and a = 0.5). The acoustic pressures of the drag dipole and lift dipole for two dimensions were non-dimensionalized by $k\sqrt{M}\sin\Theta\sqrt{a/|\boldsymbol{x}|}$ and $k\sqrt{M}\cos\Theta\sqrt{a/|\boldsymbol{x}|}$, respectively, and those for quasi three dimensions were non-dimensionalized by $kM\sin\Theta L/|\boldsymbol{x}|$ and $M\cos\Theta L/|\boldsymbol{x}|$, respectively, where $k=\rho_0\Gamma U/(4\pi a)$ and $M=U/c_0$.

As shown in Fig. 8(a), when Ut/a < -0.52, the acoustic pressure of the drag dipole (broken line) increased and that of the lift dipole decreased (solid line) as the incident vortex approached the leading edge of the airfoil. At around Ut/a = -0.52, when the incident vortex passed the leading edge (x = 0), the former pressure reached the local maximum value, and the latter reached the local minimum value. The lift dipole then continued to increase due to the increase in acceleration du/dt of the incident vortex (see Fig. 9 for du/dt and dv/dt). Near Ut/a=0.57, when the incident vortex passed the trailing edge, both pressures had local minima because the acceleration of the incident vortex also had a local minimum. These minima occurred because the path of the vortex broke near the trailing edge, as shown in Fig. 7.

As shown in Figs. 8(a) and (b), the dipoles behaved similarly in quasi three dimensions and in two dimensions. The major difference was that when the incident vortex passed the trailing edge at around t = 0.5, the acoustic pressures for both dipoles reached local minima in quasi three dimensions and two dimensions, while afterwards they reached local maxima in quasi three dimensions only. A peak at the time corresponding to the local maximum was observed in the acceleration dv/dt of the incident vortex, as shown in Fig. 9. In general, the acoustic pressure resembled the acceleration more for the quasi three dimensions than the two dimensions. The stronger resemblance occurs because the solution was obtained by integration and derivation about the time for Eq. (7) in two dimensions while only derivation about time for Eq. (11) was used in quasi three dimensions.



(a)



(b)

(a) Two dimensions; (b) Quasi three dimensions

Fig. 8. Drag and lift dipoles for NACA0012.

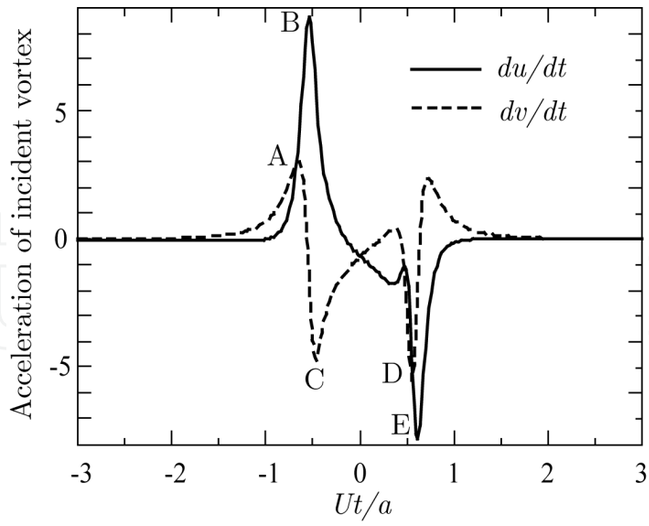


Fig. 9. Acceleration of incident vortex for two- and quasi three-dimensional analyses.

4.2 With wake vortices in non-linear motion

As stated before, Howe reported that the wake vortex shed from the trailing edge of an airfoil cancels the acoustic pressure when the Kutta condition is employed. However, his analysis was based on a linear assumption. To determine whether linearity is valid for more realistic flows with non-linear vortex movement, we conducted simulations considering the production of wake vortices that move with the velocities induced by each other. The wake vortices were produced one by one at every time step near the edge (i.e., $x = 1 + U\Delta t$ and $y = 0$), and the strength is determined by the Kutta condition, which set the strength of the bound vortex at the trailing edge at zero. The acoustic pressure was calculated by using Eq. (11) for quasi three dimensions.

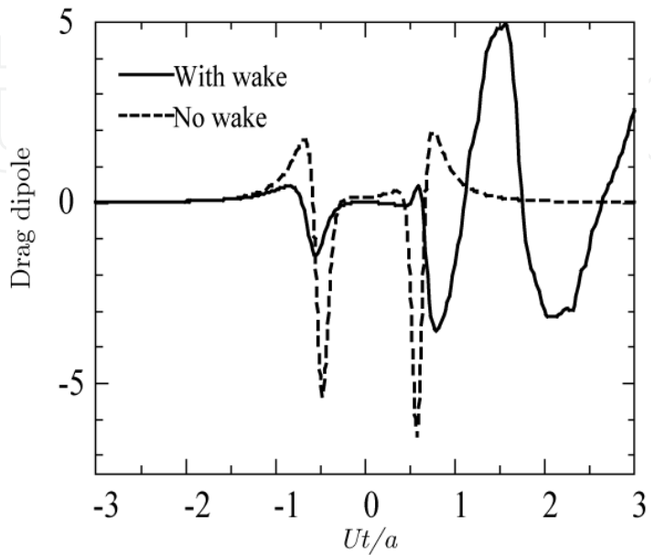
Figure 10 compares the acoustic pressures with and without the wake vortices (solid and broken lines, respectively). Before the incident vortex reached the trailing edge (Ut/a < 0.63), the peak values for the acoustic pressures of the drag and lift dipoles were smaller when the wake vortices were considered than when they were not considered. The smaller size occurs because the wake vortices decrease the acceleration of the incident vortex (Fig. 11).

After the incident vortex reached the trailing edge, the acoustic pressure without the wake vortices converged to zero, while that with the wake vortices did not, due to the continuing unsteady movements of the wake vortices.

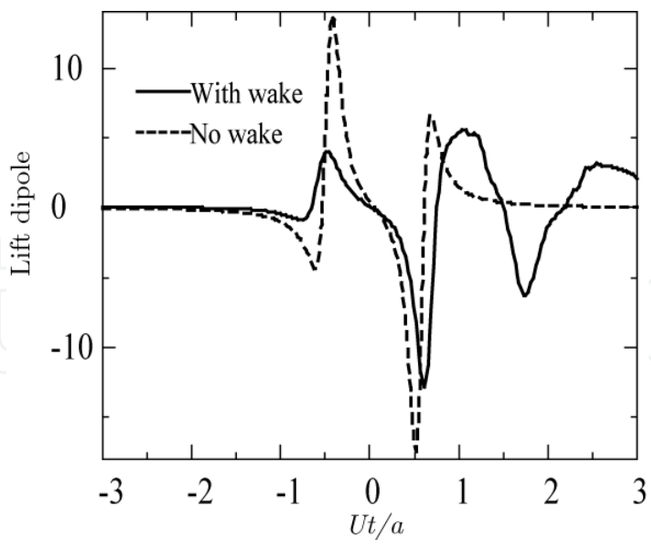
Figure 12(a) shows the wake vortices at time 7.5 when the incident vortex entraining the wake vortices passed the coordinates x = 4.4, y = -0.17. Figure 12(b) shows the path of the incident vortex. The movement looks like "hopping," and this continued to produce the acoustic pressure. When the time is very large and the position of the incident vortex is far enough from the object, the term for the incident vortex in Eq. (11) becomes

$$p(\boldsymbol{x},t) = \frac{\rho_0 L\Gamma x_1}{4\pi c_0 |\boldsymbol{x}|^2}\frac{\partial v}{\partial t} - \frac{\rho_0 L\Gamma x_2}{4\pi c_0 |\boldsymbol{x}|^2}\frac{\partial u}{\partial t} \tag{16}$$

Because the accelerations $\partial u/\partial t$ and $\partial v/\partial t$ remain sound is produced even when the incident vortex flows far away from the airfoil in the potential theory with the compact assumption. However, in a physical flow, the vortex is diffused by the viscosity or dissipated by the turbulence, so the sound disappears.



(a)



(b)

(a) Drag dipole; (b) Lift dipole

Fig. 10. Drag and lift dipoles with and without wake vortices.

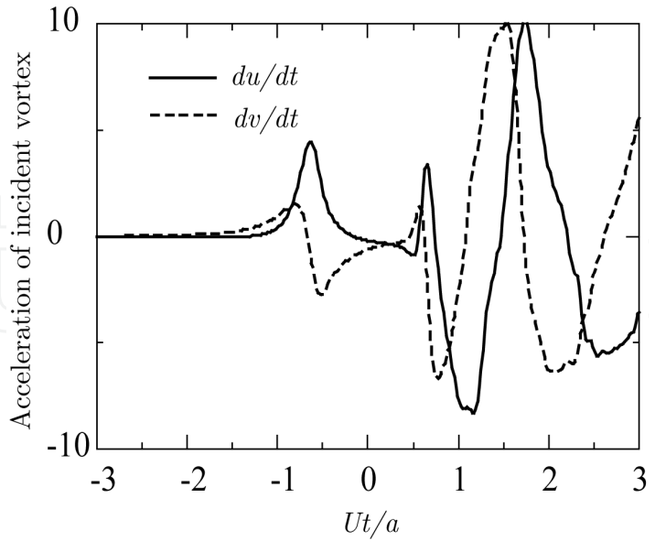
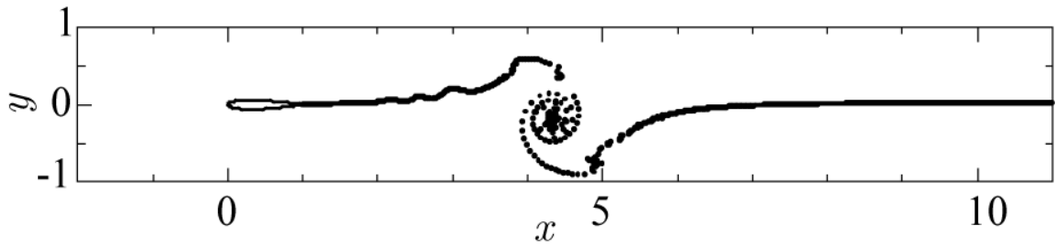
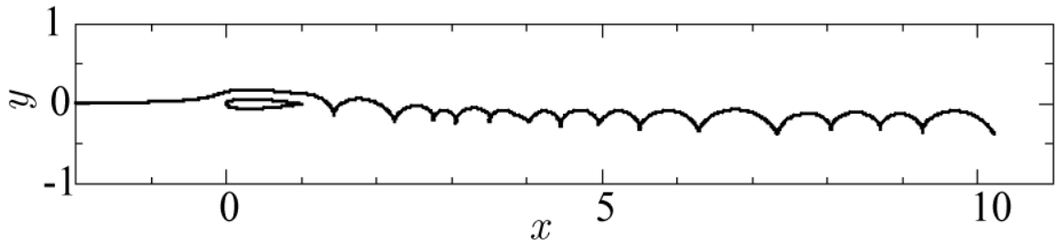


Fig. 11. Acceleration of the incident vortex with wake vortices.



(a)



(b)

(a) Wake votices at t = 7.5; (b) Path of incident vortex

Fig. 12. (a) Wake vortices and (b) path of incident vortex.

Figure 13 shows the strength of the wake vortex produced at each time step. Over most of the simulation, the strength was two orders of magnitude smaller than that of the incident vortex $\Gamma = -0.4\pi \approx -1.26$, and its maximum was 0.052, which is about 4% that of the incident vortex.

Furthermore, to examine the production mechanism of the acoustic pressure, the simulations were conducted with the incident vortex strength reduced to one-tenth of its previous value: that is, $\Gamma = -0.04\pi \approx -0.126$.

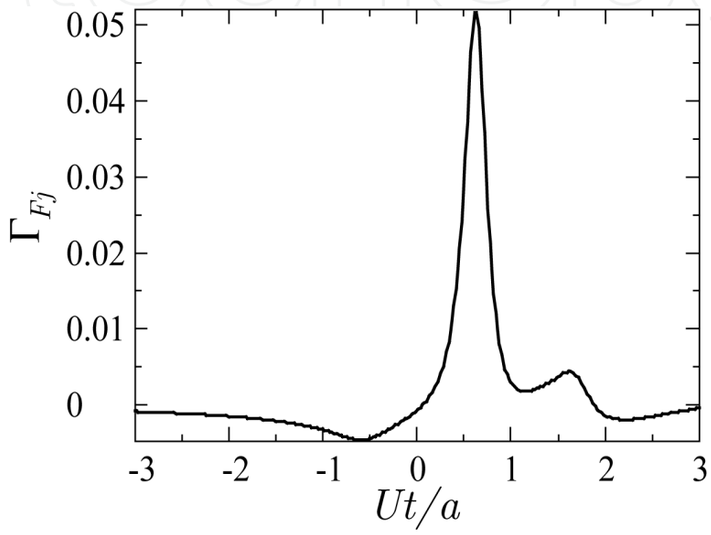
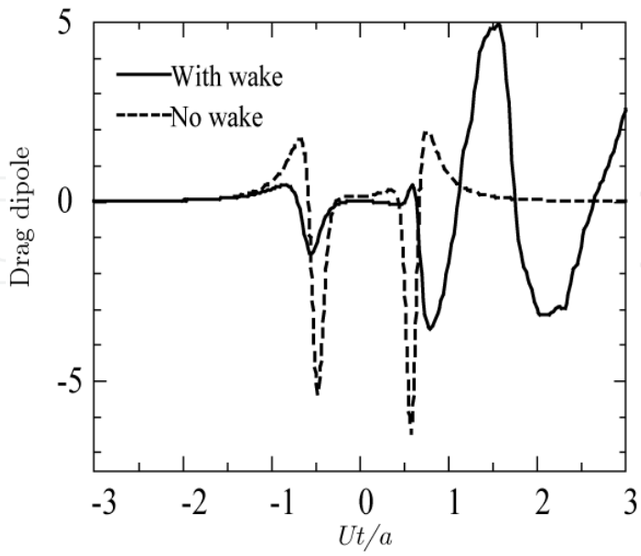


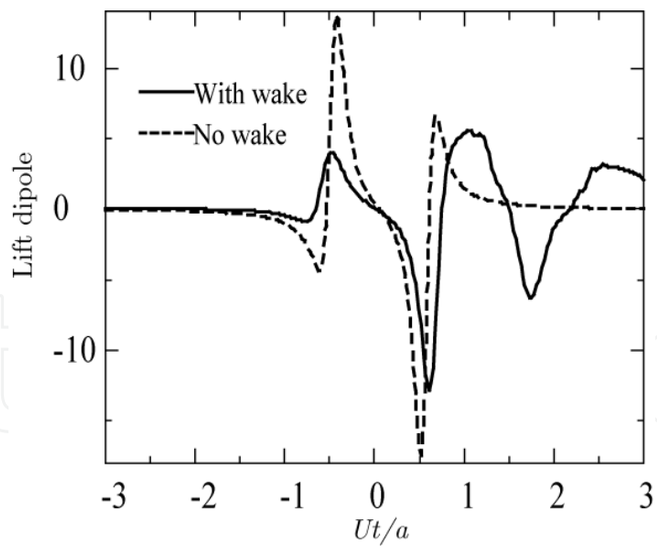
Fig. 13. Strength of wake vortices shed from trailing edge.

Figure 14 shows the acoustic pressures, with and without the wake vortices, for the drag and lift dipoles. Even though the strength of the incident vortex was decreased to one-tenth, the pressure of the drag dipole did not greatly differ from that shown in Fig. 10, while the lift dipole took a large peak value of -56.5 at time 0.75. This peak was not observed in the acceleration of the incident vortex shown in Fig. 15, so this peak was not affected by the acceleration of the incident vortex. On the other hand, the time of this peak coincides with that of the strength of wake vortices shed from the edge shown in Fig. 16. The peak value was almost 0.02, which was 16% of the incident vortex and relatively larger than the 4% in the previous simulation. The incident vortex passed the trailing edge at around time = 0.77, and the largest wake vortex was produced. This shows that the production of the wake vortex strongly affected the acoustic pressure and the acceleration of the incident vortex.

The results of our simulations show that the wake vortex shed from the trailing edge of an airfoil does not cancel the acoustic pressure. Before the incident vortex reaches the trailing edge, the pressure is decreased because of the effect of the wake vortices. However, afterwards, the movements of the wake vortices keep producing the large pressure, and the production of the wake vortices also increases the acoustic pressure.



(a)



(b)

(a) Drag dipole; (b) Lift dipole.

Fig. 14. Drag and lift dipoles for $\Gamma = -0.04\pi$

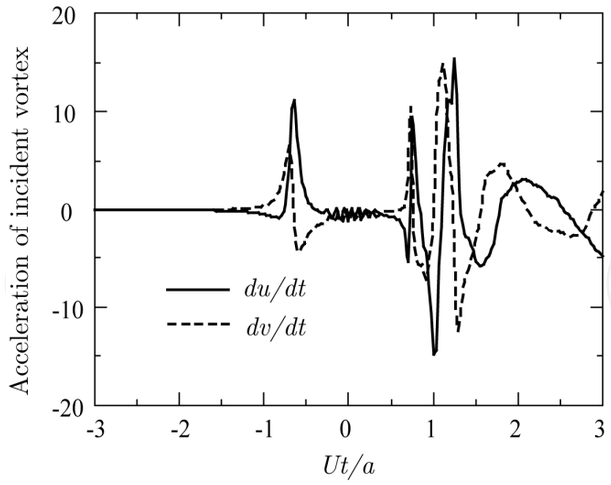


Fig. 15. Acceleration of incident vortex with the effect of wake vortices.

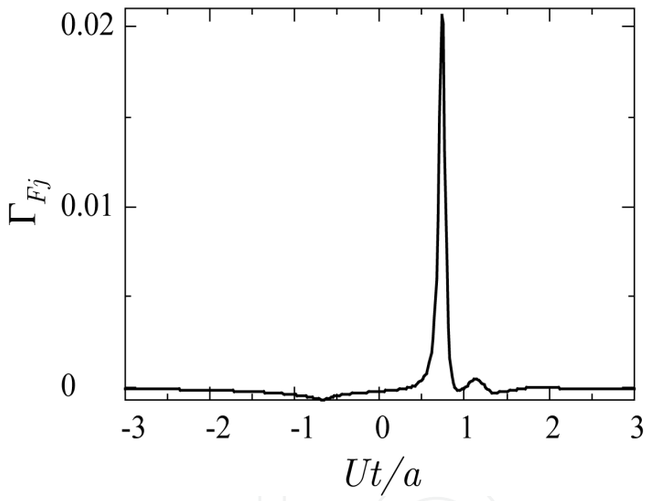


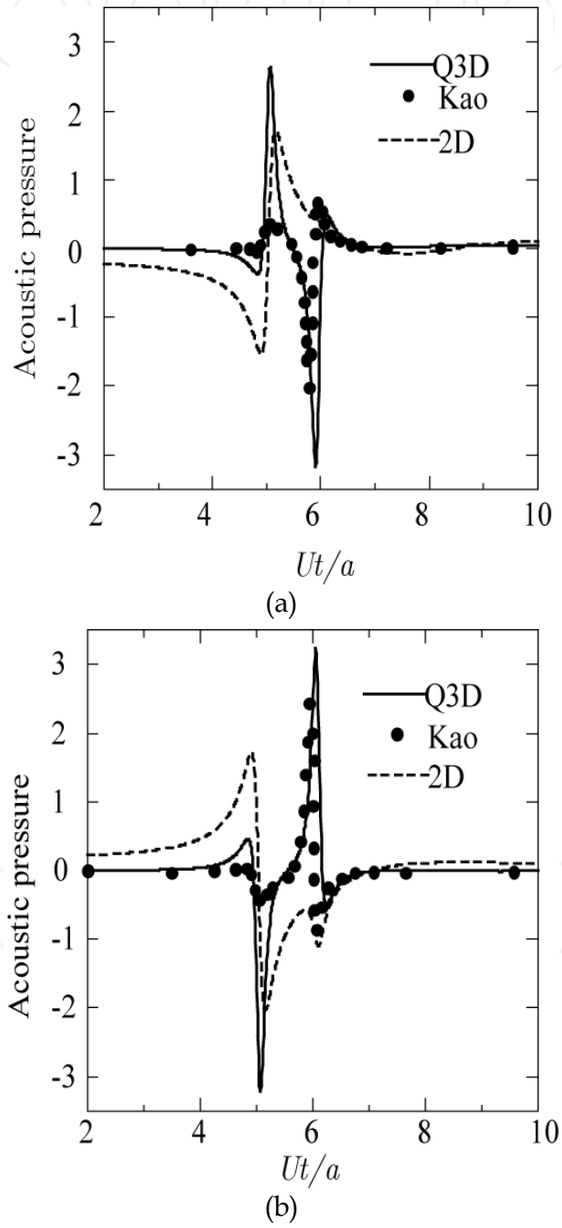
Fig. 16. Strength of wake vortices.

The reason for the disagreement may be because in Howe's analysis (1976), the wake vortices were arranged on the x axis from the trailing edge to infinity, and their strength was given by a periodic function. On the other hand, in our simulations, the wake vortices were not on the x axis but moved freely with nonlinear interaction of the vortices, and their strength was not periodic.

4.3 Comparison with asymptotic matching method

Kao (2002) studied the acoustic pressure by using the *asymptotic matching method*, which treats the near field as an incompressible fluid and the far field as a compressible fluid governed by the classical acoustic equation. The solutions in the two regions are matched asymptotically. Compared to the workload of Kao's analysis to obtain solutions, our solutions (7) and (11) are considerably simpler and easier to code.

Figure 17 compares the acoustic pressures produced by the interaction of an incident vortex, the wake vortices, and the NACA0012 airfoil as calculated by Kao (dots), the present method for quasi three dimensions (solid line), and that for two dimensions (broken line). The incident vortex of strength ± 0.1 was placed at x = -5.0, y = 0.1, and it passed above the NACA0012 airfoil located at x = 0–1. The production of the wake vortices was taken into account with the Kutta condition. Note that the strength of the incident vortex was so small that rolling up of the wave vortices was not observed, although the figure is not shown here.



(a) $\Gamma = -0.1$; (b) $\Gamma = 0.1$

Fig. 17. Comparison with the asymptotic matching method.

Although Kao's analysis was two-dimensional and we used the compact assumption that the wavelength of sound is large compared to the dimension of the solid body, the solutions by Kao agreed very well with those for the present method in quasi three dimensions. In both Kao's and our simulations, the peak was observed when the incident vortex passed the leading edge at around Ut/a = 5 and the trailing edge at around Ut/a =6.

5. Sound produced by vortex motion near a half-plane

Howe (2003) studied the sound produced by the vortex motion near a half-plane and concluded that *sound produced by the shed vortex tends to cancel the edge-generated sound attributable to the incident vortex* Γ *alone*. However, his analysis was qualitative explanation because he did not calculate the sound considering the wake vortices with nonlinear interactive movements. Therefore, we conducted simulations considering these movements.
First, we considered the flow in the ζ -plane given by the complex function for the incident vortex of strength Γ located at $\zeta = \zeta_0$, its image vortex at $\zeta = \zeta_0^*$, and the wake vortices of strength Γ_m given by

$$F = -\frac{i\Gamma}{2\pi}\log(\zeta - \zeta_0) + \frac{i\Gamma}{2\pi}\log\left(\zeta - \zeta_0^*\right) + \sum_{m=1}^{N}\frac{i\Gamma_m}{2\pi}\left(\log(\zeta - \zeta_m) - \log\left(\zeta - \zeta_m^*\right)\right) \tag{17}$$

where ζ^* is the complex conjugate of ζ . Note that the total strength of the vortices is zero. The flow about a half-plane was then obtained by transforming the flow given by Eq. (17) into the z-plane by the following conformal mapping:

$$\zeta = i\sqrt{z} \tag{18}$$

The wake vortices were shed from the edge at each time step, and the strength was determined by the Kutta condition that removes an infinite velocity at the edge. Considering this, strength Γ_N of the N-th wake vortex was calculated by the recurrence formula

$$\Gamma_N = -\frac{\sum_{j=1}^{N-1}\Gamma_j\left(\frac{(\psi_j)}{(\xi-\xi_j)^2+(\psi_j)^2}\right)}{\frac{(\psi_N)}{(\xi-\xi_N)^2+(\psi_N)^2}} \tag{19}$$

where ξ_j and ψ_j are the coordinates of the j-th free vortex (including the incident vortex) in the ζ -plane. The acoustic pressure can be calculated by applying Eq. (6.2.9) in Howe (2003) to multiple vortices.
The incident vortex of strength $\Gamma = 1$ was located at x = -20, y = 0.4, and the time step was set as 0.05. We assumed that the wake vortices were created near the edge of the half-plane (i.e., x = 0.01, y = 0) at every time step. The exact position of the edge was x = 0 and y = 0.
Figure 18 shows the results after 6000 steps. The dots represent the locations of wake vortices, and the solid line is the path of the incident vortex. The path without wake vortices considered is plotted by the broken line for comparison. The path of the incident vortex with the wake vortices was rolled up to make a spiral through the interaction with the wake vortices and lingered in a region not far from the half-plane.

Figure 19 shows the acoustic pressure produced by the interaction of the incident vortex, wake vortices, and half-plane (solid line). The acoustic pressure without wake vortices is plotted by the broken line for comparison. According to Howe, the time is non-dimensionalized as UT/l, where U is $\Gamma/(8\pi l)$ and l is the distance of the closest incident vortex to the edge (where it crosses the x-axis at time 0 in Fig. 18) when no wake vortices are considered.

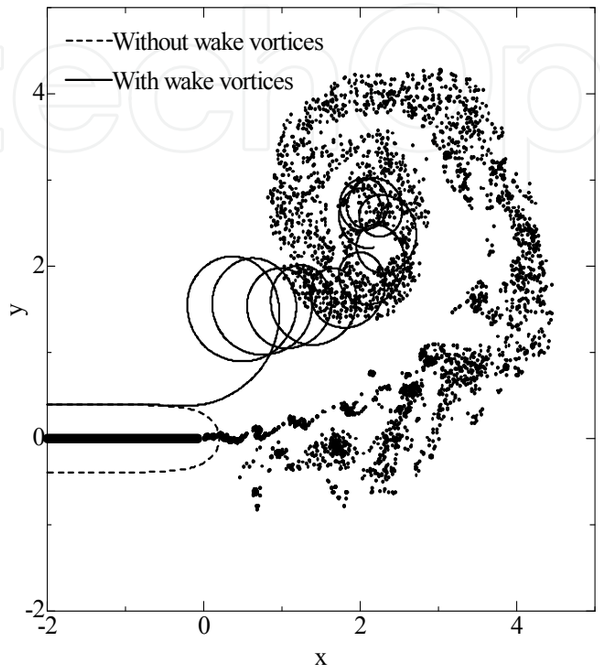


Fig. 18. Results after 6000 steps. Wake vortices (dots). Path of incident vortex with wake vortices considered (solid line). Path of incident vortex without wake vortices considered (broken line).

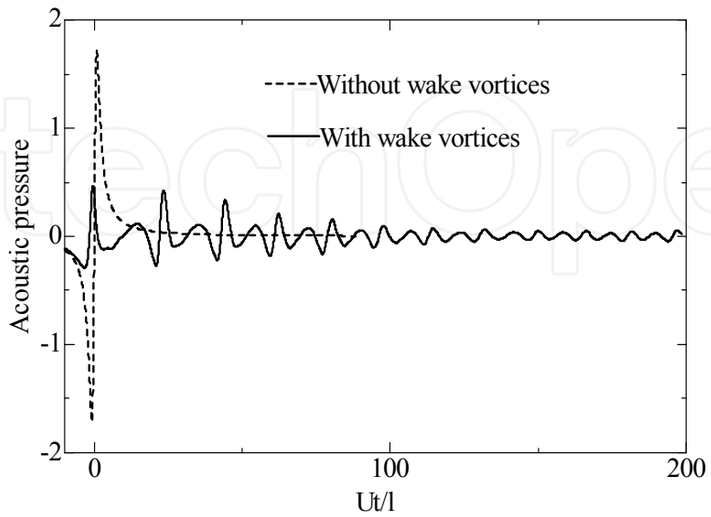


Fig. 19. Acoustic pressure. Calculated with wake vortices considered (solid line). Without wake vortices (broken line).

The peak values without wake vortices at around time = 0 were -1.72 (time = -0.790) and 1.72 (0.835), while the peak values with wake vortices were -0.29 (-3.28) and 0.47 (-0.449). This difference in values shows that the wake vortices decreased the peak values. However, the pressure continued to oscillate with the rolling movements of the incident vortex and wake vortices while it converged to zero when no wake vortices were considered.

Figure 20 shows the strength of vortices shed from the edge. When the incident vortex was far enough from the edge, wake vortices of negligible strength were produced. As the incident vortex approached the edge, the strength increased, and the wake with the largest strength of -0.0119 was produced at around time 0 when the incident vortex passed the edge. After this time, the strength of the wake vortices decreased, but oscillation due to the rolling movement was observed. The total strength of the wake vortices in Fig. 21 suddenly decreases at around time = 0, and it converged on the value of -0.9429, which is not 1 but the strength of the incident vortex. This vortex strength remains because the incident vortex did not flow away from the half-plane, and its effects on the production of wake vortices remained.

6. Three dimensions

Many factors in three-dimensional analyses affect the acoustic pressure. The effect of a change in the shape of an incident vortex on the pressure is presented here.

We considered a rectangular solid of dimensions $10\times10\times1$ with faces parallel to the x, y, and z axes with its center at the origin. An incident vortex of length 20 and strength 4π was placed from x = -10, y = -10 to x = -10, y =10 with a height of z = 0.5 in a uniform flow of speed 1. The production of the wake vortices was not considered.

The rectangular solid was represented by distributions of source and vorticity, whose strength was determined by the non-permeable condition at each time step. The surfaces of the solid were divided into 2150 panels. The bound vortices Γ_{Bi}^{j} that represent the body in the unit flow in the j direction (j = x, y and z) were obtained in advance with the non-permeable condition imposed at the center of each panel. The time step was 0.005.

Figure 22(a) shows the locations for every 50 time steps of the incident vortex flowing from the left to the right in the uniform flow without changing its shape. The velocity at which the vortex moved was calculated at the center of the vortex. Figure 22(b) shows the incident vortex, which was divided into 20 elements of the same length so that the shape of the vortex could change according to the velocity induced at each element. The shape of the vortex deformed to fit the outline of the solid, and the vortex took almost twice as much time as that shown in Fig. 22(a) to flow from the leading edge of the solid to the trailing edge.

Figure 23 compares the acoustic pressures of the drag and lift dipoles, as normalized by $\rho_0 x_1 LU\Gamma/(4\pi c_0|x|^2)$, of the rectangular solid with vortex deformation (broken line), the solid without vortex deformation (thick solid line), and, for reference, a two-dimensional flat plate from quasi three-dimensional simulation (thin solid line). Time t was normalized as Ut/a, where U is the uniform velocity of 1 and a is the half-length of the solid of 5.

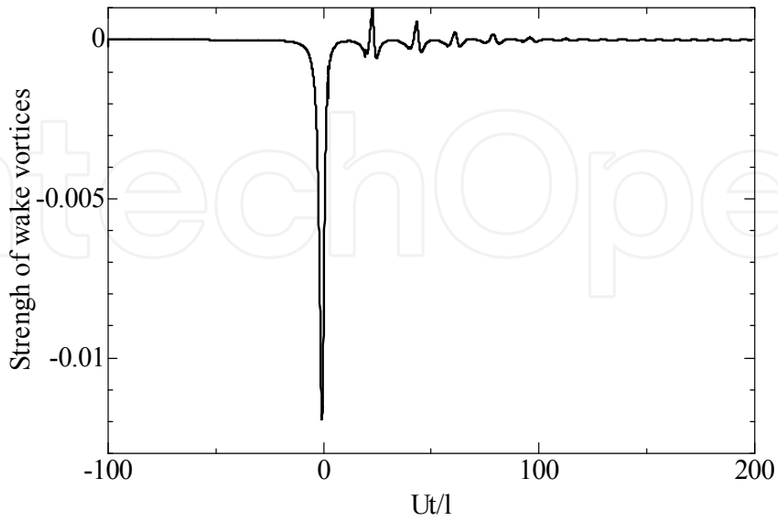


Fig. 20. Strength of wake vortices.

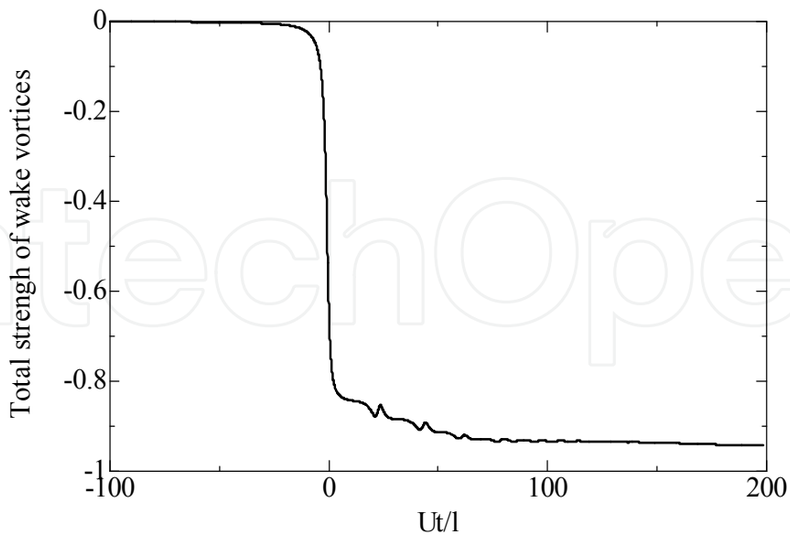
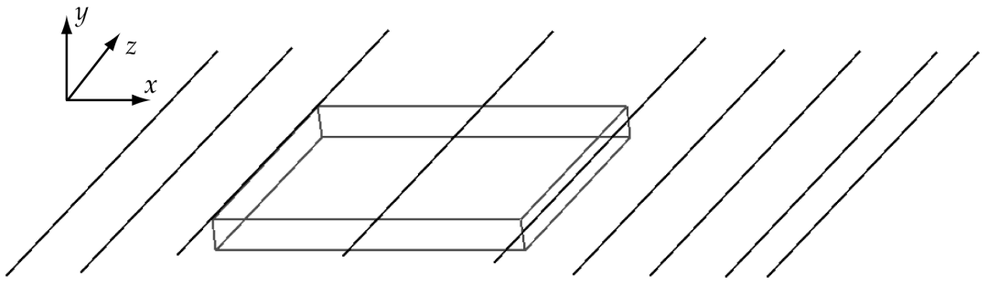
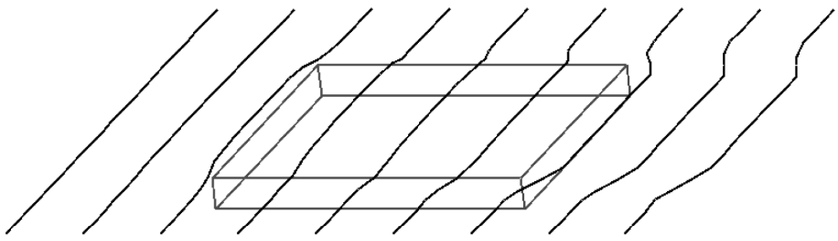


Fig. 21. Total strength of wake vortices.



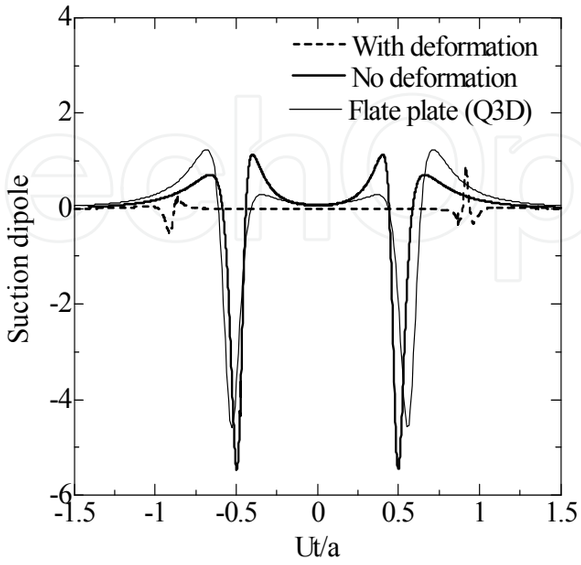
(a) Without vortex deformation



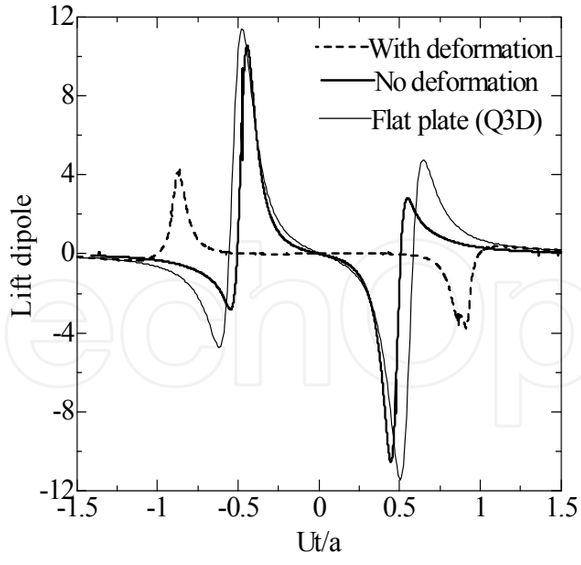
(a) With vortex deformation

Fig. 22. An incident vortex passing a rectangular solid with and without changing its shape.

(a)



(b)



(a) Drag dipole; (b) Lift dipole

Fig. 23. Comparison of acoustic pressures for rectangular solid with vortex deformation (broken line), without vortex deformation (thick solid line), and a flat plate with quasi three-dimensional simulation (thin solid line).

The pressures of the flat plate and rectangular solid without vortex deformation were similar, while these for the rectangular solid with vortex deformation were rather weakened compared with line vortex analysis without a change in shape. The reason for this was as follows: In this study, the movement of an entire vortex line without deformation was calculated using the velocity at the center of the vortex, while the movement of a vortex line, divided into multiple elements, with deformation was estimated using the velocity at each element. Accordingly, as shown in Fig. 23(a), the time period between the negative peaks was almost 1 for "No deformation" and almost 2 for "With deformation." This shows that the time period for the incident vortex to travel from the leading edge to the trailing edge in the case "With deformation" was twice the value obtained in the case "No deformation." This implied that the velocity and acceleration of the incident vortex were evaluated to be larger for the "No deformation" case than for the "With deformation" case, resulting in a decrease in the pressure with an increase in the vortex deformation, as shown in Fig. 23.

7. Conclusion

We generalized Howe's method, based on the compact assumption that the wavelength of sound is large compared to the dimension of the solid body, to treat two-dimensional shapes with unknown conformal mappings and three-dimensional obstacles. The idea for calculating the acoustic pressure of arbitrarily shaped obstacles without conformal mappings is to use three sets of bound vortices which represent the obstacles in uniform flows of speed 1 in the x and y directions in two dimensions as well as in the z direction in three dimensions. These bound vortices are obtained by the panel method in advance. The acoustic pressures obtained by our method are considerably simple and easy to code.

The results of our method for a circular cylinder agreed well with Howe's solutions, and those for an NACA0012 airfoil agreed well with Kao's solutions through the asymptotic matching method.

Although Howe reported that the wake vortex shed from the trailing edge of an airfoil or half-plane cancels the acoustic pressure when the Kutta condition is employed, our simulations showed that (1) the production of the wake vortices decreases the acoustic pressure before the incident vortex reaches the edge, (2) the non-linear movements of the wake vortices keeps producing the acoustic pressure, and (3) the production of a large wake vortex enlarges the acoustic pressure. In addition, a change in the shape of the incident vortex decreases the acoustic pressure.

The simulations conducted here were intended to show the validity and accuracy of our method and to study very fundamental problems. Applications of our method to engineering problems will be shown in the near future. In addition, a vortex method for the vortex sound without the compact assumption is the next goal.

8. References

Curle, N. (1955). The influence of solid boundaries upon aerodynamic sound, *Proceedings of the Royal Society of London*, A231, pp. 505-514

Ffowcs Williams, J. E. & Hawkings, D. L. (1969). Sound generation by turbulence and surfaces in arbitrary motion, *Philosophical Transactions of the Royal Society of London*, A264, pp. 321-342

Howe, M. S. (1976). The influence of vortex shedding on the generation of sound by convected turbulence, *J. Fluid Mech.*, Vol. 76, Part 4, pp. 771-740

Howe, M. S. (2003). *Theory of Vortex Sound*, Cambridge University Press, ISBN 0-521-01223-6

Huberson, S.; Rivoalen, E. & Voutsinas, S. (2008). Vortex particle methods in aeroacoustic calculations, *J. Comp. Physics,* Vol. 227, pp. 9216-9240

Kao, H.C. (2002). Body-Vortex Interaction, Sound Generation, and Destructive Interface, *AIAA journal*, Vol. 40, No. 4, pp. 652-660.

Ogami, Y. & Akishita, S. (2010). Numerical simulation of sound field generated by separated flows using the vortex method, *Fluid Dynamics Research,* Vol. 42, No. 1, DOI 10.1088/0169-5983/42/1/015009

Powell, A. (1964). Theory of Vortex Sound, *Journal of the Acoustical Society of America*, Vol. 36, No. 1, pp. 177-195

Sharland, I.J. (1964). Sources of noise in axial flow fans, *J. Sound Vib.*, Vol. 1, No. 3, pp. 302-322



Advanced Methods for Practical Applications in Fluid Mechanics

Edited by Prof. Steven Jones

ISBN 978-953-51-0241-0
Hard cover, 230 pages
Publisher InTech
Published online 14, March, 2012
Published in print edition March, 2012

Whereas the field of Fluid Mechanics can be described as complicated, mathematically challenging, and esoteric, it is also imminently practical. It is central to a wide variety of issues that are important not only technologically, but also sociologically. This book highlights a cross-section of methods in Fluid Mechanics, each of which illustrates novel ideas of the researchers and relates to one or more issues of high interest during the early 21st century. The challenges include multiphase flows, compressibility, nonlinear dynamics, flow instability, changing solid-fluid boundaries, and fluids with solid-like properties. The applications relate problems such as weather and climate prediction, air quality, fuel efficiency, wind or wave energy harvesting, landslides, erosion, noise abatement, and health care.

How to reference

In order to correctly reference this scholarly work, feel free to copy and paste the following:

Yoshifumi Ogami (2012). Simulation of Acoustic Sound Produced by Interaction Between Vortices and Arbitrarily Shaped Body in Multi-Dimensional Flows by the Vortex Method, Advanced Methods for Practical Applications in Fluid Mechanics, Prof. Steven Jones (Ed.), ISBN: 978-953-51-0241-0, InTech, Available from: http://www.intechopen.com/books/advanced-methods-for-practical-applications-in-fluid-mechanics/simulation-of-acoustic-sound-produced-by-interaction-between-vortices-and-arbitrarily-shaped-body-in

INTECH
open science | open minds

InTech Europe
University Campus STeP Ri
Slavka Krautzeka 83/A
51000 Rijeka, Croatia
Phone: +385 (51) 770 447
Fax: +385 (51) 686 166
www.intechopen.com

InTech China
Unit 405, Office Block, Hotel Equatorial Shanghai
No.65, Yan An Road (West), Shanghai, 200040, China
中国上海市延安西路65号上海国际贵都大饭店办公楼405单元
Phone: +86-21-62489820
Fax: +86-21-62489821

© 2012 The Author(s). Licensee IntechOpen. This is an open access article distributed under the terms of the Creative Commons Attribution 3.0 License, which permits unrestricted use, distribution, and reproduction in any medium, provided the original work is properly cited.

IntechOpen

IntechOpen